Transportation Research Part B 59 (2014) 96–116

Contents lists available at ScienceDirect

Transportation Research Part B

journal homepage: www.elsevier.com/locate/trb

Analysis of common-cause and special-cause variation in the deterioration of transportation infrastructure: A field application of statistical process control for structural health monitoring

Yikai Chen [a], David J. Corr [b], Pablo L. Durango-Cohen [c,*]

[a] Department of Civil and Environmental Engineering, Northwestern University, 2145 Sheridan Road, A320, Evanston, IL 60208, USA
[b] Department of Civil and Environmental Engineering, Northwestern University, 2145 Sheridan Road, A335, Evanston, IL 60208, USA
[c] Department of Civil and Environmental Engineering, Northwestern University, 2145 Sheridan Road, A332, Evanston, IL 60208, USA

ARTICLE INFO

Article history:
Received 20 April 2012
Received in revised form 3 November 2013
Accepted 6 November 2013

Keywords:
Transportation infrastructure
Performance modeling
Structural health monitoring
Statistical process control
Regression analysis
ARIMA-GARCH models

ABSTRACT

We present a statistical process control framework to support structural health monitoring of transportation infrastructure. We contribute an integrated, generally-applicable (to various types of structural response data) statistical approach that links the literatures on statistical performance modeling and on structural health monitoring. The framework consists of two parts: The first, estimation of statistical models to explain, predict, and control for common-cause variation in the data, i.e., changes, including serial dependence, that can be attributed to usual operating conditions. The ensuing standardized innovation series are analyzed in the second part of the framework, which consists of using Shewhart and Memory Control Charts to detect special-cause or unusual events.

We apply the framework to analyze strain and displacement data from the monitoring system on the Hurley Bridge (Wisconsin Structure B-26-7). Data were collected from April 1, 2010 to June 29, 2011. Our analysis reveals that, after controlling for seasonal effects, linear trends are significant components of the response measurements. Persistent displacement may be an indication of deterioration of the bridge supports. Trends in the strain data may indicate changes in the material properties, i.e., fatigue, sensor calibration, or traffic loading. The results also show that autocorrelation and conditional heteroscedasticity are significant sources of common-cause variation. Use of the control charts detected 43 possible special-cause events, with approximately 50% displaying persisting effects, and 25% lasting longer than one week. Analysis of traffic data shows that unusually heavy loading is a possible cause of the longest special-cause event, which lasted 11 days.

1. Introduction

Structural health monitoring (SHM) is the process of collecting and analyzing data related to the condition/properties of (subsets of elements that comprise complex) structures, such as bridges. Such data are used for a variety of purposes; however, the fundamental objective of SHM involves assessment and prediction of structural integrity, i.e., load-bearing capacity, to ensure safe and reliable operations. The most-widely used approach to achieve this objective consists of comparing

* Corresponding author. Tel.: +1 847 491 4008; fax: +1 847 491 4011.
E-mail addresses: yikai.chen@u.northwestern.edu (Y. Chen), d-corr@northwestern.edu (D.J. Corr), pdc@northwestern.edu (P.L. Durango-Cohen).

0191-2615/$ - see front matter © 2013 Elsevier Ltd. All rights reserved.
http://dx.doi.org/10.1016/j.trb.2013.11.002

measurements[1] to the predictions of a model of (immediate) structural responses to specific loading conditions. Deviations between the measurements and predictions, particularly those exceeding certain thresholds, are taken as indications of damage,[2] e.g., loads on members are too high to be supported safely. As acknowledged in the SHM literature, a fundamental limitation of this approach is that, in general, structural models (of deterioration) do not explain, and therefore cannot be used to predict, (long-term) variations in response measurements, e.g., strain, exhibited by complex structures, even when they are undamaged and operating under ordinary conditions (Sohn et al., 2002). This lack of explanatory and predictive capability hinders damage detection because it is difficult to separate damage from other sources of variation, and explains the prevalence of SHM methods to analyze structural properties that are insensitive to operational variation, including minor damage, i.e., vibration-based methods.

The objective in SHM overlaps with the literature on transportation infrastructure/asset management. The latter having a broader focus, ideally encompassing a structure's life-cycle and supply-chain, where the objective is to support a plethora of decisions, e.g., maintenance and rehabilitation, and where, in addition to safety and reliability, metrics include functional performance, i.e., ride quality, economic and environmental consequences, as well as other criteria. Statistical deterioration models have been developed to support this objective, i.e., to predict (the effect of management strategies on long-term) deterioration, and indirectly the aforementioned criteria. While, in principle, such models can be used to explain and predict measurement variations under ordinary conditions, and thereby adapted to support SHM; with few exceptions, statistical deterioration models are cross-sectional, meaning that they describe differences between facilities. This, in turn, limits their applicability to SHM, and motivates the need for methodologies capable of facility-specific (as opposed to population-level) inferences and longitudinal forecasts.

In this paper, we introduce a generally-applicable (to different types of data) statistical framework that links the two parallel streams of literature described above. The objective is to support efficient monitoring and management of transportation infrastructure. The proposed framework builds on the notion in Statistical Process Control (SPC) (cf. Shewhart, 1931; Deming, 1975) that changes in the output of a stochastic process consist of three components: **common-cause variation**, which refers to changes that can be explained, and importantly, predicted by *usual*, often observed, and recurrent operational conditions; **special-cause variation**, which refers to changes attributed to *extraordinary* events; and inherent **random variation** discussed in subsequent paragraphs. In the case of a stochastic process consisting of measurements collected from an infrastructure facility, operational conditions are those associated with traffic, weather, etc. Extraordinary events could be exogenous and even observable, such as extreme or infrequent/unique traffic or weather events, or endogenous and sometimes latent, such as the advent of certain types of damage.

Perhaps stemming from development and implementation in controlled environments, e.g., manufacturing settings where it is possible and desirable to eliminate sources of systematic variation, the focus in traditional SPC is on first, achieving, and subsequently, detecting deviations from a *state of statistical control* (SSC). In a SSC, variability is random; that is, measurements or statistics derived from a quality characteristic are assumed to be stationary, independent and identically distributed (*iid*). This variability is understood to represent the cumulative effect of many small, unavoidable causes, which explains why the Central Limit Theorem is often invoked to justify the assumption that the measurements follow a Normal Distribution (Montgomery, 2009). Occasionally, other sources of variability, i.e., special causes, alter the process of interest. In manufacturing settings, sources can include improperly adjusted or controlled machines, operator errors, or defective raw materials. Variation produced by special causes is systematic and generally large relative to random variation (Montgomery, 2009). Detection of special-cause events, therefore, consists of detecting departures from a SSC. In manufacturing settings, it is desirable, though not always possible, to identify the sources of special-cause events, i.e., *assignable causes*, in order to take corrective action.

In SHM and other settings, interventions to eliminate or correct sources of systematic variation may be (physically/politically) impossible or undesirable, meaning that such variability may be present throughout the data, i.e., it constitutes common-cause variation. The effect of temperature on response measurements, e.g., strain, is a relevant example in the SHM context. As explained by Alwan and Roberts (1988), in such situations, the SPC focus is narrowed (from reaching a SSC) to the detection of special-cause events. To achieve this objective they propose the following two-part framework, which we adapt to support SHM:

1. Formulation and estimation of statistical models to explain and predict common-cause variation. These models allow for inferences based on the measurements, as well as for forecasting their progression under usual operating conditions. It is this analysis, therefore, that allows decision-makers/agencies to be proactive in terms of planning interventions. Importantly, these models are also used to control for, i.e., remove, common-cause variation from the data. The resulting *standardized innovations*, i.e., prediction errors, constitute the fundamental input to the second part of the framework, consisting of:

[1] Measurements can be replaced with surrogates, i.e., damage-sensitive features, obtained by processing the data.

[2] Wenzel (2009) defines damage as changes to material or geometric properties of a structure, including changes to the boundary conditions and connectivity. Damage affects current or future performance of such systems, i.e., load-bearing capacity. Herein, deterioration refers to the damage initiation and progression process.

2. Use of control charts to detect special-cause events. This analysis provides a rigorous statistical basis to react to measurements that do not conform to those collected under ordinary conditions. In an online monitoring setting this could lead to scheduling (equipment or structural) inspections, road closures, etc. In a *post hoc* analysis context, detection of special-cause events provides forensic capabilities, e.g., to identify precursor events contributing to (major) damage. Also, as is discussed in Section 4.3, special-cause event detection could lead to refinements of statistical performance models.

We use the framework to analyze strain and displacement data from the SHM system installed on the Hurley Bridge (Wisconsin Structure B-26-7). Our implementation differs from Alwan and Roberts (1988) in that rather than using a pure time-series method to control for common-cause variation, we use a two-stage approach. First, we estimate regression models to control for variability in the measurements that can be related to changes in explanatory variables: ambient and steel temperature, humidity and traffic. Such an approach, not uncommon in time-series analysis, is attractive from an engineering perspective because it provides structured understanding of (the effect of different sources of variability on) the underlying process.[3] The analysis reveals significant seasonal effects, as well as small, but significant linear trends, which indicate permanent, systematic displacements. Such trends in the strain measurements could be related to changes in the material properties, e.g., fatigue, sensor calibration, or loading conditions. In the second stage, we use ARIMA-GARCH models, a class of time series models, to control for serial dependence not explained by the regression models, i.e., in the residuals. Our analysis shows that serial dependence is a significant source of unexplained, common-cause variation. Modeling serial dependence, therefore, leads to improved explanation of the progression of the measurement sequences. Importantly, as shown in Appendix B, failure to control for serial dependence can lead to unreliable detection of special-cause events.

Our implementation of the second part of the framework uses Shewhart and Memory Control Charts to detect special-cause variation not explained by the aforementioned statistical models. Our analysis of the ARIMA-GARCH standardized innovations reveals 43 possible special-cause events over the analysis period. Approximately 50% of these events had persisting effects on the response measurements lasting at least 3–4 days, with 25% lasting at least one week. We analyze weigh-in-motion data to illustrate the process of identifying possible causes of these events, and show that unusually heavy loading is a possible cause of the longest special-cause event, which lasted 11 days.

1.1. Contributions and organization

Fundamentally, the work contributes a statistical framework that links (i) the literature on SHM, focused on detection and analysis of special-cause events (caused by damage), with (ii) the literature on statistical deterioration modeling to support transportation infrastructure/asset management, focused on explaining and predicting common-cause variation. The integration is predicated on methodological developments that constitute significant advances/departures to the literature in both fields. Specifically:

- The paradigm dominating the development of methods to support SHM of bridges and other complex structures is highly-specific to the analysis of structural vibrations. We discuss these methods further in Section 2. At this point, we highlight that, unlike other properties/measurements, modal parameters characterizing the vibrations are stationary and (relatively) insensitive to operational variation and even to minor damage (Farrar et al., 2005). This obviates the need (for continuous monitoring) to explain and predict common-cause variation, and simplifies damage-detection because raw measurements exceeding certain thresholds tend to be indicators of (special-cause events caused by) damage. In contrast, and motivated by recent developments in SHM technologies that allow for high-frequency/continuous, long-term monitoring of a variety of structural properties, the proposed framework begins by explaining and predicting common-cause variation, including deterioration when damage is a permanent source of variation in the data. As shown in our example application, this is not only appealing, but also necessary for the reliable detection of special-cause events. Thus, the proposed approach fills an acknowledged void in the SHM literature (Sohn et al., 2002), and has the potential to generalize its focus from the analysis of vibrations to other structural response measurements.
- As stated earlier, with few exceptions, statistical deterioration models are cross-sectional, which limits their applicability to SHM, and motivates the need for methodologies capable of facility-specific (as opposed to population-level) inferences and longitudinal forecasts. Models overcoming fundamental obstacles, such as unobserved heterogeneity (Archilla and Madanat, 2000; Prozzi and Madanat, 2001; Chu and Durango-Cohen, 2008a) and autocorrelation (Madanat et al., 1997; Chu and Durango-Cohen, 2007; Chu and Durango-Cohen, 2008a), have recently been published; however, additional statistical analysis is still needed. The work herein is a step in this direction. For example, to the best of our knowledge, we present the first model of conditional heteroscedasticity, i.e., time-varying volatility, in the deterioration of transportation infrastructure.
- While the use of GARCH has become commonplace in applied econometrics (Engle, 2001), Fang and Zhang (1999); Ord (2009), and the work herein are among the few reported applications for SPC.

[3] This approach had been used for SPC by Mandel (1969) and others, who introduce residual control charts, and serve as the foundation for the framework of Alwan and Roberts (1988).

- Limitations of previous work that motivate the proposed framework can be partly attributed to poor data availability/adequacy. The use of high-quality field data to validate the framework is, therefore, an important contribution from an engineering perspective.

The remainder of the paper is organized as follows: In Section 2 we review and position our work with respect to the literature on SHM systems, and on statistical performance models to support transportation infrastructure/asset management. In Section 3, we describe the use of statistical models and control charts to, respectively, explain/control for common-cause variation, and to detect special-cause events. In Section 4, we present an extensive empirical study to illustrate the capabilities of the proposed framework. The section includes a detailed description of the data, as well as the results of our implementation of both parts of the framework. We conclude in Section 5 by summarizing our main findings and discussing directions for future research.

2. Related work

In this section, we position the proposed framework with respect to the literature on SHM systems, and with respect to statistical performance models developed to support transportation infrastructure/asset management.

2.1. Overview of SHM systems

Vibration-based methods are the most widely-researched techniques to assess the structural integrity of bridges (and other structures). Vibrations induced by operational or environmental loads, or by mechanical devices in the case of lab specimens, are analyzed to detect damage. These methods rely on the premise that a structure's response, i.e., modal parameters such as resonant frequencies, mode shapes and modal damping are functions of the physical properties of the structure, i.e., mass, damping and stiffness, and that changes, e.g., reductions in stiffness resulting from the onset of cracks or loosening of a connection, cause detectable changes in the modal parameters characterizing the vibrations (Doebling et al., 1998). Depending on the structure and loading conditions, these parameters can be obtained analytically or empirically. Modal parameters are stationary and (relatively) insensitive to operational variation, including minor damage (Farrar et al., 2005). This provides a lot of flexibility because it reduces the need for continuous monitoring and for modeling common-cause variation. Additional advantages of vibration-based methods are that they have simple requirements in terms of instrument type, i.e., accelerometers, and location. Flexibility in locating instruments facilitates deployment of tethered instruments, which enable data and power transmission, and explains the (historical) appeal of these methods for field applications. As a pioneering example, we cite Vincent (1962b); Vincent (1962a) who analyzed the vibrations of the Golden Gate Bridge. Data were collected with accelerometers that were installed in 1945 and operated until 1954.

Technological advances in the last two decades have motivated the development and adaptation of instruments, equipment, as well as data processing and analysis methods for SHM. The literature documenting these efforts is vast and growing rapidly. As a starting point, we refer the reader to Balageas et al. (2006), who review and classify SHM systems. Lynch (2007); Rice et al. (2011) are examples documenting recent developments. In addition to technological issues, these papers describe protocols for data acquisition, transmission, and methods for distributed data processing. Notably what has improved is sensor reliability, i.e., quality of data acquisition, enabling continuous, long-term, simultaneous monitoring of various properties, which motivates the need to develop rigorous and computationally-efficient methods with general applicability to process different data types emanating from multiple sources.

The sophistication of SHM systems relates to characteristics of the algorithms used for data processing and analysis. At a high-level, two approaches have emerged: structural and statistical. In the first approach, measurements are compared to the predictions of a reference model of structural responses to certain, typically short-term, loading conditions.[4] Deviations between the measurements and predictions, particularly those exceeding certain thresholds, are taken as indications of damage, e.g., loads on members are too high to be supported safely. Fritzen (2005) provides a recent overview of ancillary analytical and computational methods used to infer location, type and magnitude of damage. Analytical methods have performed well at characterizing damage in controlled environments, e.g., lab specimens or (rotating) equipment in manufacturing settings (Wowk, 1991). In terms of field applications, Friswell and Mottershead (1995) describe finite-element model updating, perhaps, the most promising technique. This technique involves calibrating a finite-element model of the structure with measurements collected for a reference, "undamaged" state. Subsequent deviations between measurements and predictions, lead to model updating to achieve agreement, and in turn, shed light on plausible damage scenarios: location, type and magnitude. As stated earlier, a significant limitation of this approach is that, in general, structural models of (long-term) damage progression are not rich enough to adequately explain common-cause measurement variations exhibited by complex structures, and motivates the need to develop suitable analytical methods to monitor, explain and predict the progression of measurements/properties.

Statistical methods, referred to as *pattern recognitions approaches* in the literature (Kiremidjian, 2009), are used to analyze variations in the (progression of) measurements. This literature overlaps with the proposed analysis of special-cause variation. Limitations of this work are related to the data used for analysis, which correspond to measurements from controlled

[4] For example, Li et al. (2001); Xu et al. (1997), respectively, characterize vibrations induced by traffic or by environmental loads, including a cyclone.

experiments in lab settings where specific damage types are purposely induced, e.g., The ASCE Benchmark Structure (Johnson et al., 2004). Various methods, including control charts (Sohn et al., 2000; Fugate et al., 2001) and clustering algorithms (Nair and Kiremidjian, 2007), have been tested to identify and evaluate damage scenarios. In virtually all cases, an original, undamaged lab-specimen/structure yields stationary, *iid* response measurements. Lynch et al. (2006) is a notable exception in that the data are from a field implementation; however, the focus of the work is the adaptation of technology and the establishment of innovative (distributed) data processing and communications protocols. In summary, the performance of these methodologies requires further testing in field applications and with measurements, where common-cause variation is significant, where instead of controlled damage scenarios, there are multiple, potentially-unknown sources of special-cause variation, including damage, and where their effect can be transient. These difficulties are acknowledged in the literature (Sohn et al., 2002), and serve as motivation for our work.

2.2. Overview of statistical performance models to support transportation infrastructure/asset management

Statistical models developed to support the management of transportation infrastructure focus on characterization of common-cause variation. Arguably, this literature starts with AASHO Road Test (AASHO, 1962), a large-scale, accelerated pavement deterioration test. Comprehensive reviews of the condition assessment and forecasting literature can be found in McNeil et al. (1992); Hudson et al. (1997); Gendreau and Soriano (1998); Van Noortwjk and Frangopol (2004). Madanat et al. (1995); Madanat and Wan Ibrahim (1995); Madanat et al. (1997); Mishalani and Madanat (2002); Frangopol et al. (2001) are examples of models developed for bridges or components, and are related to the proposed research. Aside from predicting deterioration, the objective is to estimate the effect of structural design, maintenance, traffic, or environmental conditions, including their interactions, on various performance criteria, including damage initiation and progression, functional, economic or environmental impact. These models are often used to support resource allocation decisions. Due, in part, to (historical) difficulties and costs of collecting long-term data, as well as theoretical and practical problems rendering time-series models unappealing,[5] the overwhelming majority of these models are cross-sectional, meaning that they describe differences between facilities. This limits their applicability for SHM where the objective is to make facility-specific (as opposed to population-level) inferences and longitudinal predictions. These and other technical issues are described in Chu and Durango-Cohen (2007); Chu and Durango-Cohen (2008a), who introduced the use of state-space specifications of time-series models to estimate pavement performance models. Here, we present developments to refine the capabilities of these models. In particular, to the best of our knowledge, we present the first model of time-varying volatility in the infrastructure deterioration context.

3. Methodology

The proposed SHM framework builds on Alwan and Roberts (1988) and consists of two parts: (i) formulation and estimation of statistical models to explain, predict and control for common-cause variation; and (ii) control chart analysis of the ensuing standardized innovations, i.e., prediction errors, to detect special-cause events. In this section, we first outline and justify our approach to analyze common-cause variation. We then describe the use of control charts as a rigorous statistical approach to detect special-cause events.

3.1. Statistical modeling framework

As described in Section 2.2, numerous statistical methods have been used to explain and predict common-cause variation in performance/response data from infrastructure facilities. While there is significant flexibility in the choice of method, specification, estimation approach, etc., rigorous deployment of the proposed SHM framework depends on generating prediction errors that are *iid* Normal, i.e., that comply with the assumptions underlying the use of control charts. For simplicity, in Section 4.2, we develop a two-stage approach to model common-cause variation. The first stage consists of formulation and estimation of commonly-specified multilinear regression models to explain the (contemporaneous) effect of exogenous variables on the response measurements. The ensuing models are appealing and allow for a meaningful decomposition of the response measurements. The second stage involves estimation of ARIMA-GARCH models to capture serial dependence in the regression residuals. While not as intuitive as regression models, as is shown in the analysis, the use of ARIMA-GARCH models to control for serial dependence is essential for the reliable detection of special-cause events. Because the analysis depends on the data, and because the underlying tools are not uncommon in transportation research, details, including the model specifications and assessment, are relegated to the analysis presented in Section 4.2.

In terms of justifying the approach, we note that sequential (as opposed to simultaneous) estimation of regression and time-series models simplifies the process, but has the potential to introduce bias stemming from partitioning the estimation problem. It also is relevant to mention that the estimation of regression models with serially dependent residuals is incongruent with the underlying assumptions of classical linear regression. Nevertheless, the use of regression constitutes a

[5] Pure time-series models can be unattractive because they do not include exogenous explanatory variables: design characteristics, traffic, environment, maintenance, etc. Furthermore, the variables that are included (autoregressive or moving average terms) can provide adequate predictions, but can be difficult to interpret physically.

widely-used pre-processing step in time series analysis (Alwan, 2000; Brockwell and Davis, 2002, pp. 11–15, 210–211). As is the case in the present study, the objective is to control for variation, excluding carryover effects, that can be attributed to explanatory variables, including trends. Therefore, in spite of the aforementioned bias potential, we find the results to be acceptable and appealing.

3.2. Control charts

In this section, we first present a broad overview of the use of control charts to detect special-cause events, followed by a detailed description of the control charts and supplementary runs rules used in the analysis presented in Section 4.3.

Control charts are graphical displays of the evolution of quality characteristics over time. They provide a statistical basis to detect special-cause events, which result in departures from a random process generating (Normal) *iid* data – an SSC where appropriate. Various control charts and supplementary runs rules have been designed to test for particular types of departures. To illustrate, we present a generic control chart in Fig. 1 following Montgomery (2009).

In the example, x_t is a random variable, with mean μ_x and standard deviation σ_x, that represents a (sample) statistic from a quality characteristic measured at time $t = 1, \ldots, T$. In addition to displaying the time series, $\{x_t\}_{t=1}^{T}$, control charts include reference levels: a Center Line (CL) set at μ_x, Upper and Lower Control Limits (UCL and LCL) set at $\mu_x \pm L\sigma_x$. L, a distance from the CL measured in multiples of the process standard deviation, is chosen so that measurements outside the control limits, i.e., *outliers*, indicate possible departures from the assumption of *iid* measurements, i.e., changes in the mean or increases in the variance of the process. It is common practice to set $L = 3$, which means that for measurements following a Normal Distribution, an assumption/approximation justified by the Central Limit Theorem, the probability that a measurement from a random process falls outside of the control limits is 0.0027 (0.00135 in each direction). The choice of L trades off the probability of Type I and Type II errors, α and β. Type I errors, false positives, arise when one incorrectly concludes that the process has deviated from stationary, *iid* behavior, whereas Type II errors, false negatives, arise when deviations are not detected. For a Normal *iid* process, $\alpha = 0.0027$ ($\sim$ 3 outliers per 1,000 measurements), which means that the expected number of measurements between outliers is $1/\alpha = 370.4$. β, of course, depends on the nature and magnitude of the departure from the nominal data-generating process. Using a larger L decreases Type I, but increases Type II errors.

In the remainder of the section, we describe the specific charts and supplementary runs rules used in Section 4.3 to detect special-cause variation.

3.2.1. Shewhart control charts

We consider two types of Shewhart Control Charts: Individual and Moving Range Control Charts, respectively, to monitor deviations in the mean and variance of various response measurements.

3.2.1.1. Individual control chart. Individual Control Charts are used to monitor the central tendency in the measurement sequences. The chart's center line (CL) corresponds to the sample average – an unbiased estimate of the mean value of the measurements:

$$\mathrm{CL} = \hat{\mu} = \bar{x} = \frac{1}{T}\sum_{t=1}^{T} x_t \tag{1}$$

We follow common practice in SPC and set $L = 3$ to specify the upper and lower control limits: UCL and LCL. This choice yields $\alpha = 0.0027$. Following Montgomery (2009), an unbiased estimate of the process standard deviation, $\hat{\sigma}$, is obtained as follows:

$$\hat{\sigma} = \frac{\overline{\mathrm{MR}}}{d_2} \tag{2}$$

where $\mathrm{MR}_t = \mid x_t - x_{t-1} \mid$ is the individual moving range for the pair of consecutive measurements at time $t-1$ and t, and $\overline{\mathrm{MR}} = \frac{\sum_{t=2}^{T}\mathrm{MR}_t}{T-1}$ is the mean individual moving range. When 2 consecutive measurements are used to calculate the moving ranges, $d_2 = 1.128$.

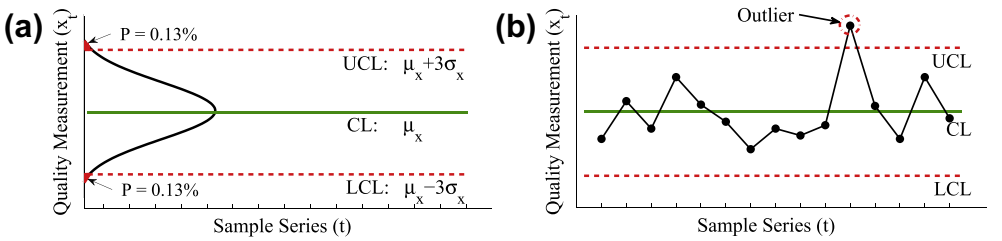

Fig. 1. Generic control chart: (a) sample probability distribution, (b) conceptual example.

3.2.1.2. Moving range control chart. Moving Range Control Charts are used to monitor the variance in the measurement series. The reference levels are as follows:

$$\mathrm{CL} = \overline{\mathrm{MR}} \tag{3}$$

$$\mathrm{UCL} = D_4 \cdot \overline{\mathrm{MR}} \tag{4}$$

$$\mathrm{LCL} = D_3 \cdot \overline{\mathrm{MR}} \tag{5}$$

where D_4 and D_3 are parameters that depend on the number of measurements used to calculate the moving ranges, MR_t. The control limits are designed so that interpretation of the chart is analogous to the Individual Control Chart. For moving ranges constructed from 2 consecutive measurements:

$$D_4 = 1 + 1.5\sqrt{2\pi - 4} = 3.27$$

$$D_3 = 1 - 1.5\sqrt{2\pi - 4} = -1.27$$

Since D_3 is negative, the lower control limit is set to zero, and thus moving ranges are only compared to the UCL. For measurements above UCL, $\alpha = 0.009$. A practical implication of a negative LCL value is that the control chart has diminished capabilities to detect reductions in variation.

3.2.2. Supplementary runs rules

In addition to outliers, supplementary rules have been designed to detect aberrant sequences, i.e., deviations from *iid* measurements, in Shewhart Charts. Different rules provide different capabilities, i.e., they are used to test different hypotheses about the process generating the data. In this paper, we consider 4 of the runs rules given by Nelson (1984) and apply them to the Individual Control Charts: rule N2 triggers an alert when 9 consecutive measurements fall on one side of CL; rule N3 triggers an alert when 6 consecutive measurements are increasing or decreasing; rule N6 triggers an alert when 4 out of 5 consecutive measurements fall beyond 1σ from CL on the same side; and rule N7 triggers an alert when 15 consecutive measurements fall between $\pm 1\sigma$ from CL. Rules N2, N6 and N7 are designed to detect sustained shifts in the mean (N2) or variance (N6 and N7) of the process. Rule N3 is designed to detect sustained drifts in the process mean (or variance).[6] Montgomery (2009) elaborates on these issues and provides additional information about the capabilities of supplementary runs rules.

Following Duncan (1986), assuming Normal *iid* data, the corresponding Type I errors of N2, N3, N6 and N7 can be analytically determined: $\alpha_{N2} = 0.0039, \alpha_{N3} = 0.0028, \alpha_{N6} = 0.0043$ and $\alpha_{N7} = 0.0033$. Under the (strong) assumption of independence, Duncan (1986) uses the following expression to calculate the overall Type I error rate for simultaneous implementation of multiple runs rules:

$$\alpha = 1 - \prod_{k=1}^{K}(1 - \alpha_k) \tag{6}$$

where α_k is the Type I error rate of the kth rule ($k = 1, 2, \ldots, K$). Thus, Eq. (6) suggests that use of the aforementioned supplementary runs rules with the Individual Control Chart results in $\alpha \approx 0.0169$, i.e., Normal *iid* data are expected to trigger about 17 warnings per 1,000 measurements (over a 5-fold increase compared to outlier detection alone). The expected number of measurements between warnings decreases from 370.4 to 59.2.

3.2.3. Memory control charts

When monitoring infrastructure, detection of small magnitude (sustained) shifts or drifts is of interest. Our conjecture is that such changes may constitute early indications of damage. Importantly, such changes are not always identifiable by Shewhart Control Charts because the statistics monitored only reflect the sample information in that period, i.e., they are memoryless. In turn, this motivates the implementation of control charts with memory properties. Here, we present two such charts to monitor mean and variance: the Exponentially Weighted Moving Average (EWMA) Chart, and the Exponentially Weighted Root Mean Square (EWRMS) Chart.

3.2.3.1. EWMA control chart. The EWMA Control Chart employs a scheme in which the statistic being monitored, EWMA_t, is a weighted average of the current measurement, x_t, and the history of the process collected in $x_{t-1}, x_{t-2}, \ldots$. The EWMA statistic at each period is defined as:

$$\mathrm{EWMA}_t = \lambda \cdot x_t + (1 - \lambda) \cdot \mathrm{EWMA}_{t-1} \tag{7}$$

where $0 < \lambda \leqslant 1$ is a tuning parameter that is used to control the chart's sensitivity. More weight is assigned to the most recent observation with the remaining weight steadily decreasing for earlier observations. EWMA_0 is set to $\bar{x}$. If the original measurements, $\{x_t\}_{t=1}^{T}$, are independent random variables with constant variance, σ^2, then the standard deviation of EWMA_t corresponds to:

[6] Shifts refer to sudden/discrete changes, whereas drifts refer to gradual/continuous changes.

$$\sigma_{\mathrm{EWMA}_t} = \sigma \cdot \sqrt{\frac{\lambda}{2-\lambda}\left[1-(1-\lambda)^{2t}\right]} \tag{8}$$

Thus, the levels in an EWMA Control Chart are set as follows:

$$\mathrm{CL} = \bar{x} \tag{9}$$

$$\mathrm{UCL}_t = \bar{x} + 3\sigma \cdot \sqrt{\frac{\lambda}{2-\lambda}\left[1-(1-\lambda)^{2t}\right]} \tag{10}$$

$$\mathrm{LCL}_t = \bar{x} - 3\sigma \cdot \sqrt{\frac{\lambda}{2-\lambda}\left[1-(1-\lambda)^{2t}\right]} \tag{11}$$

where an unbiased estimate of σ is as shown in Eq. (2). Moreover, since $0 < \lambda \leqslant 1,\ (1-\lambda)^{2t}$ converges quickly to 0 as t increases. Therefore the control limits converge to:

$$\mathrm{UCL} = \bar{x} + 3 \cdot \frac{\overline{\mathrm{MR}}}{d_2} \cdot \sqrt{\frac{\lambda}{2-\lambda}} \tag{12}$$

$$\mathrm{LCL} = \bar{x} - 3 \cdot \frac{\overline{\mathrm{MR}}}{d_2} \cdot \sqrt{\frac{\lambda}{2-\lambda}} \tag{13}$$

3.2.3.2. EWRMS control chart. Detecting small magnitude, persistent shifts or drifts in a process's variance is also of interest. Moreover, as discussed in Alwan (2000), Moving Range Control Charts have weaknesses[7] that motivate the development of EWRMS Charts as a robust and appealing approach to monitor dispersion. The corresponding statistics are defined as follows:

$$\mathrm{EWMS}_t = \lambda \cdot (x_t - \mu)^2 + (1-\lambda) \cdot \mathrm{EWMS}_{t-1} \tag{14}$$

$$\mathrm{EWRMS}_t = \sqrt{\mathrm{EWMS}_t} \tag{15}$$

where EWMS_t is a statistic called exponentially weighted mean square. The control limits for the EWRMS Control Chart as follows:

$$\mathrm{UCL} = \frac{\overline{\mathrm{MR}}}{d_2} \cdot \sqrt{\frac{\chi^2_{\frac{\phi}{2}f}}{f}} \tag{16}$$

$$\mathrm{LCL} = \frac{\overline{\mathrm{MR}}}{d_2} \cdot \sqrt{\frac{\chi^2_{1-\frac{\phi}{2}f}}{f}} \tag{17}$$

where $\chi^2_{\frac{\phi}{2}f}$ and $\chi^2_{1-\frac{\phi}{2}f}$ denote the $100(\frac{\phi}{2})$ and $100(1-\frac{\phi}{2})$ percentile point of the Chi-Square Distribution with f degrees of freedom. The degrees of freedom are a function λ:

$$f = \frac{2-\lambda}{\lambda} \tag{18}$$

4. Empirical study

In this section, we use the framework described earlier to estimate statistical performance models to explain common-cause variation, and control charts to detect special-cause variation, for structural response measurements collected from the Hurley Bridge.

4.1. Data

The data for the study are from the SHM system operating on the Hurley Bridge (Wisconsin Structure B-26-7). The bridge carries westbound traffic on US Route 2 over the Montreal River from Ironwood, Michigan to Hurley, Wisconsin. The bridge consists of 3 spans that are supported by a steel structure consisting of five girders with a composite deck. The SHM system was designed, installed and operated by the Infrastructure Technology Institute (ITI) at Northwestern University in collaboration with the Wisconsin Department of Transportation (WisDOT) (Kosnik, 2010). The development of the SHM system was motivated by WisDOT's concern that loads associated with logging trucks traveling from Michigan into Wisconsin are causing premature deterioration of the structure. One of the specific concerns is related to excessive movement.

[7] (i) Setting LCL = 0 inhibits the chart from detecting reductions in variation. (ii) Successive moving-range are correlated due to the overlapping calculation. (iii) The underlying distribution of the moving ranges is highly skewed and non-negative. Thus, the assumption/approximation of Normal data tends to be strong.

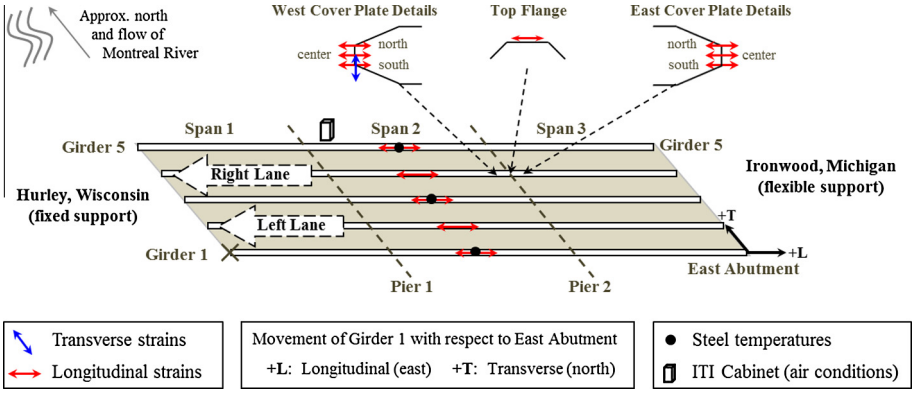

Fig. 2. Schematic of the Hurley Bridge.

In terms of instrumentation, the SHM system includes 2 displacement transducers, and 13 strain gages that are used to evaluate the responses of structural elements to exogenous factors: traffic and environment. In addition, the SHM system has instrumentation to measure ambient temperature and humidity, as well as temperature on the steel girders. A weigh-in-motion system, located upstream (East) of the bridge, provides information about traffic loads. A schematic of the bridge, including sensor identification and location, is presented in Fig. 2. We also use the figure to specify our conventions regarding frame-of-reference and directions, i.e., displacements are measured with respect to Girder 1's support on the East abutment; East and North correspond to the positive longitudinal and transversal directions, respectively.

In terms of the design of the SHM system, the displacement transducers are placed at the location subject to the greatest (expected) movement. The girder supports on the Wisconsin side (West) are fixed, whereas the supports on the Michigan side (East) are flexible (rollers). There are two vehicle lanes on the bridge deck, and Girder 4 serves as the major support for the right lane where most of the truck traffic is expected. In turn, this explains the large number of strain gages at critical points on this girder. For reference, strain gages were installed on each of the 5 girders at the mid-point of Span 2. Additional details regarding the instrumentation, including the labels that we use to identify each of the measurements, appear in Table 1.

The data used in the empirical study were collected between April 1, 2010 and June 29, 2011, for an analysis period of length $T = 455$ days. Measurements, both response and exogenous, were collected at a frequency of 100 Hz. Hourly averages are transmitted by a computer on-site, which we use to construct and process averages for each day in the analysis period. Thus, we construct a time-ordered series of 455 data points for each measurement.[8] Data from the weigh-in-motion system includes information about every vehicle traversing the bridge during the analysis period, an average of 5200 vehicles/day.

4.2. Analysis of common-cause variation

We use the two-stage modeling approach outlined in Section 3.1 to analyze common-cause variation in the response data. In Section 4.2.1, we describe the formulation and estimation of a set of commonly-specified multilinear regression models to explain the effect of the exogenous variables on the response measurements. In Section 4.2.2, we describe the formulation and estimation of ARIMA-GARCH models to capture and control for serial dependence in the residuals of the regression models.

4.2.1. Multilinear regression models

We use regression analysis to explain the effect of the exogenous variables on the structural response measurements. For simplicity, we specify a common equation for each of the 15 measurements. The models also include linear trend terms as supplementary predictors. Prior to specifying the common equation, we investigated the multicollinearity among the predictor variables using the Variance Inflation Factor Method. The analysis led to the removal of ambient temperature from the regression Eqs. (A). In addition, preliminary analysis did not yield a model where (cumulative) traffic effects were statistically-significant, and thus, traffic was also excluded as an explanatory variable.[9] The regression equations were, therefore, formulated as follows:

$$y_t^m = \beta_0^m + \beta_1^m t + \beta_2^m \text{Humid}_t + \beta_3^m \text{ST}_t + \epsilon_t^m \tag{19}$$

[8] The optimal treatment of temporal resolution among measurements can be complex. We adopt a homogeneous specification here for simplicity. Despite the ensuing limitations, we find it good enough for our objective in this paper to control for common-cause variation and detect special-cause events.

[9] One plausible explanation is that the transmission of average hourly response measurements (and the construction of daily averages) filters the effect of traffic loads (on the strain measurements). Notwithstanding, for the purpose of this analysis, the exclusion provides a set of events that could be related to special-cause variation.

Table 1
Instrumentation on the Hurley Bridge.s

	Instrument	Measurement	Unit	Element	Location	Axis
Structural responses	Displ-L	Displacement	mils	Girder 1	East abutment	Long.
	Displ-T					Trans.
	G1-S2-M			Girder 1	Span 2, mid-point	Long.
	G2-S2-M			Girder 2	Span 2, mid-point	Long.
	G3-S2-M			Girder 3	Span 2, mid-point	Long.
	G4-S2-M			Girder 4	Span 2, mid-point	Long.
	G5-S2-M			Girder 5	Span 2, mid-point	Long.
	G4-P2-TF			Girder 4 top flange	Pier 2	Long.
	G4-WCP-SL	Strain	μstrain		Pier 2, west end south edge	Long.
	G4-WCP-ST				Pier 2, west end south edge	Trans.
	G4-WCP-CL				Pier 2, west end center	Long.
	G4-WCP-NL			Girder 4 bottom	Pier 2, west end north edge	Long.
	G4-ECP-SL			flange cover plate	Pier 2, east end south edge	Long.
	G4-ECP-CL				Pier 2, east end center	Long.
	G4-ECP-NL				Pier 2, east end north edge	Long.
Exogenous	ST-G1			Girder 1	Span 2, mid-point	
	ST-G3	Steel	°F	Girder 3	Span 2, mid-point	
	ST-G5	temperature		Girder 5	Span 2, mid-point	
	Temp	Air temperature	°F			
	Humid	Relative humidity	%			

where $t = 1, \ldots, 455$ and $m = 1, \ldots, 15$ are, respectively, used to index the days in the analysis period, and each of the 15 measurements. The variables Humid_t and ST_t, respectively, correspond to the average relative humidity and the average steel temperature on day t. The steel temperature corresponds to that of the girder closest to the relevant instrument (temperature on Girder 1 was used for measurements on Girder 2, and temperature on 3 for measurements on 4). The coefficients β_0^m and β_1^m represent the intercept, and the slope of the linear trend in measurement sequence m, respectively. We use ϵ_t^m to denote the residuals.

The estimation results are presented in Table 2. For each coefficient, β_j^m, a t-stat larger than 1.97 (d.f. = 453) indicates that the corresponding variable is statistically-significant at a 95% confidence level. Coefficients not deemed statistically-significant are enclosed in parentheses. In terms of goodness-of-fit, the models for the following measurements resulted in high R^2 values: Displ-L (Longitudinal displacement), Displ-T (Transverse displacement), G4-P2-TF (Longitudinal strain on the top flange of Girder 4), and G4-WCP-ST (Transverse strain on the bottom flange cover plate of Girder 4, west end south edge). The vast majority of the variance in these measurements, over 85%, is explained by corresponding changes in the exogenous variables together with the linear trend. The models obtained for the other measurements show lower, though reasonable levels of fit with R^2 values ranging from 40% to 70%. Basic data transformations did not lead to significant improvements in the goodness-of-fit, which means that either the relationships between measurements and explanatory variables are more sophisticated, or that additional variables are needed to explain changes in the measurements. These directions are not the focus of this paper, so they are not explored further.

Examination of the estimates presented in Table 2 indicates that linear trends are significant component of all of the measurement sequences, with relatively higher magnitude in the longitudinal directions. Physically, the results mean that, over the analysis period, Girder 1 is drifting to the North and East at average speeds of 0.03 and 0.22 mils/day.[10] This movement is in excess to the movement associated with variation in the explanatory variables, and is a likely indication of deterioration of the fixed supports on the Wisconsin (West) side of the bridge. In the case of the strains, small, but significant, linear trends could indicate changes in the material properties, e.g., fatigue, the sensor calibration, or the loading conditions. In terms of the effect of the exogenous factors, we observe that increased humidity leads to reduction in longitudinal strains while increased steel temperature leads to the opposite effect with the exception of the West Cover Plate. We also observe that the transverse strain (G4-WCP-ST) consistently shows opposite trends than the longitudinal measurements on the same plate. In terms of overall interpretation, the analysis allows for an intuitive decomposition of the measurement sequences into *level*, given by the intercepts in Eq. (19), *linear trend* (second term), *seasonality* (third and fourth terms), and *error* components (residuals). As an example, Fig. 3 provides a graphical representation of such decomposition for the transverse displacement measurements (Displ-T). The residuals are presented at the bottom of the figure. In terms of interpretation, recalling that Displ-T corresponds to the instrument's position relative to the support/abutment (in the transverse direction), we observe that during summer, the bridge moves North; whereas in the winter the bridge moves South. After controlling for the error, the net position is drifting to the North at a rate of 0.03 mils/day.

For simplicity, in the remainder of the paper, we focus our analysis on Displ-L, Displ-T, G4-P2-TF and G4-WCP-ST, the four measurements whose variance was largely explained by changes in the exogenous variables. In addition, we also selected two strains from the mid-point of Span 2, G1-S2-M and G4-S2-M, which is a critical location on the bridge. These strains

[10] 1 mil = 10^{-3} in.

Table 2
Multilinear regression: parameter estimates.

Measurement	Level		Linear trend		Relative humidity		Steel temperature		R^2 (%)
	β_0	t-stat	β_1	t-stat	β_2	t-stat	β_3	t-stat	
Displ-L	4762.1	473.3	0.22	27.6	(0.01)	(0.13)	7.28	135.7	97.8
Displ-T	4192.3	563.8	0.03	4.82	0.22	2.9	1.97	49.7	86.0
G1-S2-M	460.4	54.9	0.14	21.1	−0.64	−7.5	0.70	15.7	56.1
G2-S2-M	414.2	61.4	0.12	21.8	−0.73	−10.6	0.74	20.5	64.0
G3-S2-M	206.6	26.5	0.14	22.9	−0.94	−11.7	1.04	25.7	70.9
G4-S2-M	−127.4	−19.0	0.13	23.1	−0.65	−9.3	1.04	28.6	72.4
G5-S2-M	132.7	16.9	0.13	20.9	−0.90	−11.2	0.47	11.3	55.0
G4-P2-TF	561.1	219.7	0.08	39.4	−0.20	−7.5	0.85	63.1	91.2
G4-WCP-SL	416.2	32.5	0.13	12.9	−1.85	−14.2	−0.34	−5.0	44.3
G4-WCP-ST	127.7	31.3	−0.02	−4.9	0.38	9.0	0.99	46.4	85.6
G4-WCP-CL	−217.3	−15.8	0.21	18.9	−1.84	−13.2	(−0.03)	(−0.4)	51.7
G4-WCP-NL	897.4	76.0	0.13	13.5	−1.63	−13.5	−0.21	−3.5	43.1
G4-ECP-SL	−252.0	−26.1	0.16	20.6	−1.15	−11.7	0.79	15.5	58.9
G4-ECP-CL	18.9	2.1	0.14	20.2	−0.85	−9.3	0.69	14.5	55.2
G4-ECP-NL	−142.3	−15.4	0.15	21.1	−0.95	−10.1	0.86	17.7	60.3

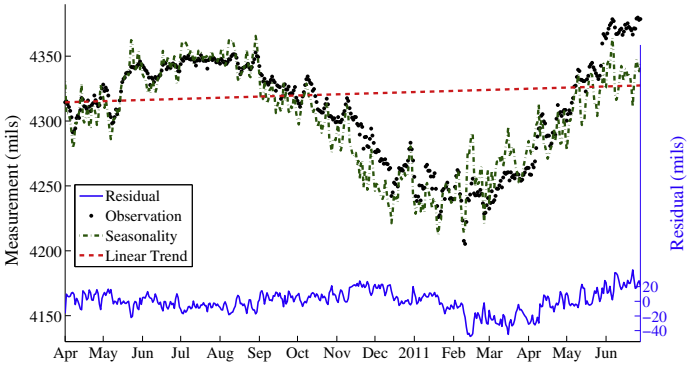

Fig. 3. Structural decomposition: transverse displacement (Displ-T).

are from the same girders as the other measurements, which provides redundant detection and assessment capabilities. Collectively, the analysis of the 6 measurements provide a reasonable sample to illustrate the proposed framework. Complete results appear in Chen (2013).

4.2.2. Time series models

In this section, we present ARIMA-GARCH models, a class of time series models, to analyze serial dependence that is not captured in the regression models presented in the previous section. From an engineering perspective, regression models are appealing because variations in a measurement sequence are related to changes in the explanatory variables. The inclusion of intercept terms in the regression Eq. (19) yields sequences of residuals, each with zero mean, capturing unexplained variation. Serial-dependence, i.e., carryover effects from earlier measurements, possibly influenced by earlier changes in the explanatory variables, can be a significant source of unexplained common-cause variation. Modeling serial dependence, therefore, leads to refinements in forecasting the progression of the measurement sequences. Moreover, the analysis of special-cause variation (Section 4.3) is predicated on the assumption of randomness, and, in turn, motivates the need to control for sources of systematic variation, such as serial dependence. In B, we illustrate the pitfalls of ignoring serial dependence in the analysis of special-cause variation. In the remainder of the section, we describe statistical tests and the ARIMA-GARCH framework to identify and control for serial dependence. We use the transversal displacement, Displ-T, as a representative example, and report the results of our analysis for the other 5 measurements.

Serial dependence in the regression residuals is quantified by analyzing the corresponding Autocorrelation Functions (ACF's). In Fig. 4, we present ACF's for the residuals of Displ-T. For any lag $\geqslant 1$, stationary and serially-independent time series yield ACF's with small values (in magnitude), i.e., the ACF values should fall between the confidence bounds[11] superimposed in Fig. 4. The values of the ACF in Fig. 4, however, decay slowly (as a function of lag), which indicates an autocorrelated and non-stationary residual series. In addition, it is important to check if a similar dependence in the variance of the residual

[11] The confidence bounds correspond to ± 2 standard deviations from the mean. A point between the bounds indicates that the auto-covariance of the series at this time-lag is statistically negligible with approximately 95% confidence.

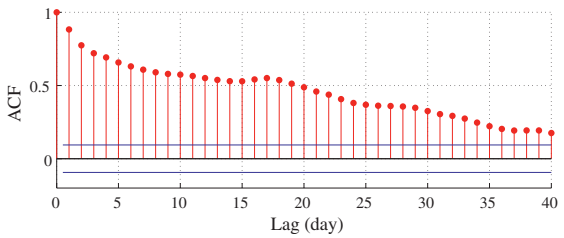

Fig. 4. Autocorrelation functions of Displ-T regression residuals.

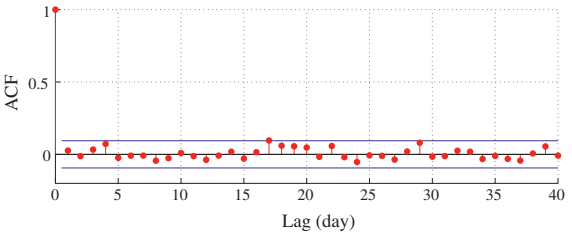

Fig. 5. Autocorrelation functions of Displ-T standardized innovations.

series exists. Such dependence, referred to as a Generalized Autoregressive Conditional Heteroscedasticity (GARCH) effect, indicates time-varying volatility. Through the Engle Hypothesis Test (Engle, 2001), we confirmed the presence of such GARCH effect at a 95% significance level for each measurement.

We use an ARIMA-GARCH model, Eqs. (20)–(23), to model serial dependence in the mean and variance of the residual series. The first step, i.e., the "integrated" part of the framework, is to construct stationary series by differencing. Application of the Kwiatkowski-Phillips-Schmidt-Shin (KPSS) Test suggests that first-order differences, shown in (20), are sufficient for each of the m residual series. In the second step, we use MLE to find the ARMA-GARCH coefficients, in (21)–(23), that capture serial dependence in the ensuing series.

$$z_t^m = \epsilon_t^m - \epsilon_{t-1}^m \tag{20}$$

$$z_t^m = \sum_{i=1}^{p} \psi_i^m \cdot z_{t-i}^m + \theta_0^m + e_t^m + \sum_{j=1}^{q} \theta_j^m \cdot e_{t-j}^m \tag{21}$$

$$e_t^m = x_t^m \cdot \sigma_t^m, \quad x_t^m \sim iidn(0,1) \tag{22}$$

$$\left(\sigma_t^m\right)^2 = \sum_{k=1}^{r} a_k^m \cdot \left(\sigma_{t-k}^m\right)^2 + b_0 + \sum_{l=1}^{s} b_l^m \cdot \left(e_{t-l}^m\right)^2 \tag{23}$$

where ϵ_t^m corresponds to the time t regression residual of measurement sequence m, z_t^m is the first-order difference. Eq. (21) is an AutoRegessive Moving Average (ARMA) model where z_t^m is a linear combination of its historic values, $z_{t-1}^m, \ldots, z_{t-p}^m$, and the associated error terms, $e_t^m, \ldots, e_{t-q}^m$. Each error term e_t^m, in turn, consists of a time-dependent standard deviation, σ_t^m, and white noise, x_t^m. Eq. (23) is the GARCH (Generalized Autoregressive Conditional Heteroscedasticity) part capturing the dependence in the series variances. It relates $(\sigma_t^m)^2$ to its historic values, $(\sigma_{t-1}^m)^2, \ldots, (\sigma_{t-k}^m)^2$, and previous squared error terms, $(e_{t-1}^m)^2, \ldots, (e_{t-l}^m)^2$. Satisfactory model estimation yields a standardized innovation series, $\{x_t^m\}_{t=1}^T$, where $x_t^m = e_t^m/\sigma_t^m$ follows a Standard Normal Distribution $(N(0,1))$. The orders of the ARMA and GARCH components, $p,\ q,\ r,\ s$, are selected so that the standardized innovations series, $\{x_t^m\}$, satisfy the normality assumption, and so that they do not display autocorrelation or conditional heteroscedasticity. Unfortunately, the coefficients in the models, $\psi,\ \theta,\ a,\ b$, do not lend themselves to intuitive, physical explanations. The Kolmogorov–Smirnov Test and the Engle Test (at 95% confidence levels) were used to verify compliance with the randomness and normality assumptions.[12] As an intuitive example of the validity of the assumptions, Fig. 5 shows the ACF's associated with the standardized innovations for Displ-T.

In the order-selection process, we use the Partial Autocorrelation Function (PACF) of the observations series z_t^m as a benchmark. For example, if the PACF's of z_t^m fall within the confidence bounds for all time-lags $\geqslant 3$, we start with an ARMA $(2, 2)$ specification and reduce the orders until the above criteria are violated. The Engle test provides an initial estimate of r and s in the GARCH specification. After the orders are determined, we use MLE to find the coefficients $\psi_i^m,\ \theta_j^m,\ a_k^m$ and b_l^m.

[12] These statistical tests also serve to verify compliance of the standardized innovation series with the assumptions underlying the control charts used to detect special-cause events. We emphasize that compliance with these assumptions does not mean that the series are void of outliers or aberrant sequences.

Parameters estimates, intercepts omitted, for the ARMA-GARCH models for each of the 6 measurement sequences are presented in Table 3.

4.3. Analysis of special-cause variation

In this section, we use Shewhart and Memory Control Charts described in Section 3.2.1,3.2.2 and 3.2.3 to detect variation in the measurement sequences that is not explained by the statistical models presented earlier. First, we illustrate the construction of control charts by analyzing the transverse displacement (Displ-T). We then summarize the results and insights from our analysis of the other measurement sequences. Finally, we describe our use of the weigh-in-motion data, excluded in the development of statistical models, to identify traffic-loading events that might have contributed to special-cause variation.

4.3.1. Shewhart control charts

We consider two types of Shewhart Control Charts: Individual and Moving Range Control Charts to, respectively, monitor the mean and variance of the standardized innovation series, $\{x_t^m\}_{t=1}^T$. To simplify the presentation, the superscript m is omitted. Fig. 6 shows the Individual and Moving Range Control Charts for Displ-T, which led to the detection of 5 and 8 out-of-control points, respectively. Because only 1 (or 2) outliers are expected in 455 measurements from a stationary, *iid* process, the 5 outliers detected suggest the presence of special-cause events leading to changes in the mean of the data-generating process. Interpretation of the Moving Range Control Chart needs to account for the dependence between consecutive MR_t, which means that outliers may reflect changes in the process mean (as opposed to the variance). Readers are referred to Crowder (1987) for additional details.

Fig. 7 shows implementation of the supplementary runs rules of Nelson (1984). Rules N2 and N6 suggest a persistent downward shift in the process mean during February 2011 that lasted for about 10 days. Rule N2 detected a downward shift in the process mean at the end of December 2010 which also lasted 10 days. Rule N3 detected a downward drift in the process mean starting in the end of March 2011, as well as an upward drift in May 2011 with respective durations of 7 and 6 days. Finally, rule N7 detected a decrease in the variance of data occurring in January 2011. Again, the larger than expected number of warnings suggest the presence of special-cause variation.

4.3.2. Memory control charts

Fig. 8 presents EWMA Control Charts for Displ-T with decreasing values of λ. When $\lambda = 1$, the EWMA Chart is equivalent to the Individual Control Chart, showing 5 outliers (Fig. 8(a)). Setting $\lambda = 0.5$, smooths out the outliers, and directs the attention to the out-of-control event in February 2011 (Fig. 8(b)). At $\lambda = 0.1$ and $\lambda = 0.02$, all of the signals, except for the one in February 2011 (Fig. 8(c) and (d)), disappear. This is evidence of a persistent shift of Girder 1 to the South lasting 8–11 days.

The tuning parameter in the EWMA control chart can be customized in the range $0 < \lambda \leqslant 1$. The smaller its value, the smoother the resulting chart with an increased focus on detecting persistent changes in the mean as opposed to outliers. The choice of λ depends on the desired performance characteristics of the chart. For instance, it can be designed to detect a desired magnitude shift. Interested readers are referred to Crowder (1989) and Lucas and Saccucci (1990). Common ranges

Table 3
ARMA-GARCH: parameter estimates.

Measurements	ARMA						GARCH			
	ψ_1	t-stat	ψ_2	t-stat	θ_1	t-stat	a_1	t-stat	b_1	t-stat
Displacements:										
Displ-L	0.48	9.6			−0.95	−55.5	0.95	41.1	0.036	2.5
Displ-T	0.73	11.5	−0.19	−3.8	−0.85	−19.1	0.96	41.2	0.026	1.8
Strains:										
G1-S2-M	0.38	5.8			−0.87	−25.4	0.80	7.8	0.089	2.0
G4-P2-TF	0.60	11.1			−0.94	−42.3	0.93	19.3	0.045	1.8
G4-WCP-ST	0.42	6.0			−0.85	−21.6	0.94	38.5	0.046	2.6
G4-S2-M	0.34	5.0			−0.85	−22.8	0.97	29.5	0.021	1.5

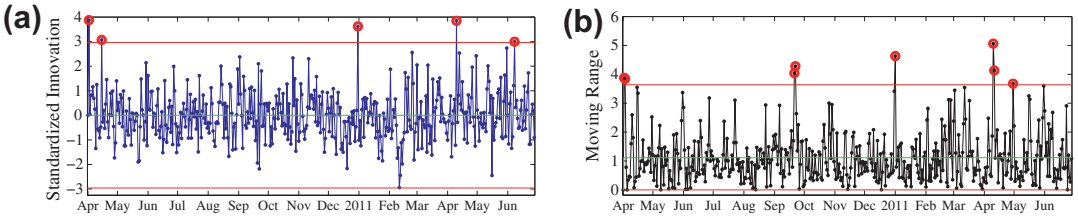

Fig. 6. Shewchart control charts for Displ-T: (a) individual, (b) moving range.

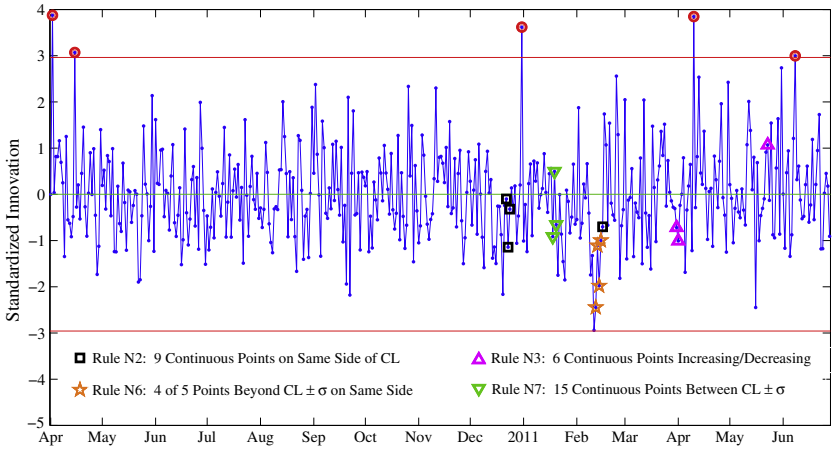

Fig. 7. Individual control chart for Displ-T with supplementary runs rules.

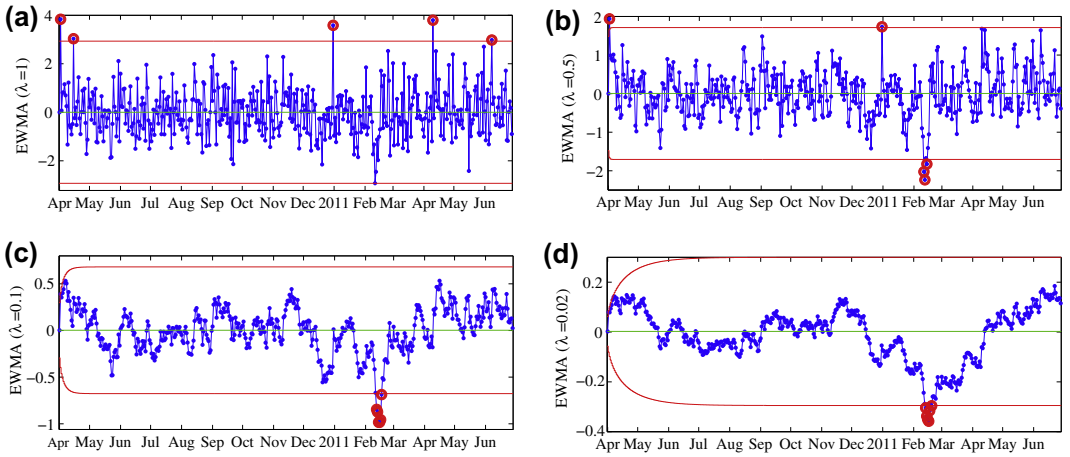

Fig. 8. EWMA control charts for Displ-T: (a) $\lambda = 1$, (b) $\lambda = 0.5$, (c) $\lambda = 0.1$, (d) $\lambda = 0.02$.

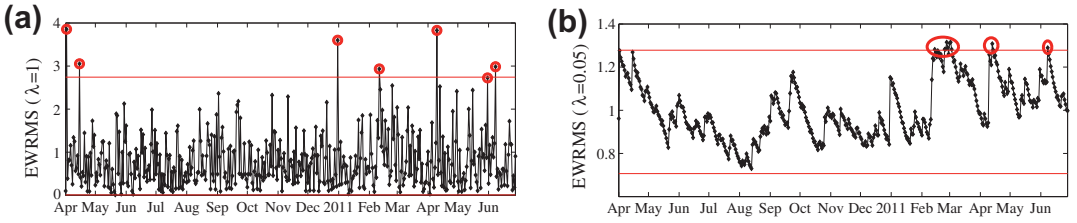

Fig. 9. EWRMS control charts for Displ-T: (a) $\lambda = 1$, (b) $\lambda = 0.05$.

of λ are 0.05 to 0.25. Here, we use four values of λ on the EWMA chart of Displ-T to illustrate the chart's sensitivity. In our analysis of the 6 measurements, we found that setting $\lambda = 0.1$ generated meaningful results.

Fig. 9 presents our implementation of the EWRMS Chart for Displ-T with weight parameter λ decreasing from 1 to 0.05. When $\lambda = 1$, the chart detects 7 outliers over the analysis period. Setting $\lambda = 0.05$ has a smoothing effect. Attention is focused on events that have a persistent effect.

4.3.3. Analysis of other measurements

We present Individual, Moving Range, EWMA and EWRMS Control Charts for the other 5 measurement sequences. For simplicity, consistency, and due to space limitations, we present EWMA Charts with $\lambda = 0.1$, and EWRMS Charts with $\lambda = 0.05$. Fig. 10 shows the results for Displ-L, Fig. 11 for G1-S2-M, Fig. 12 for G4-P2-TF, Fig. 13 for G4-WCP-ST, and

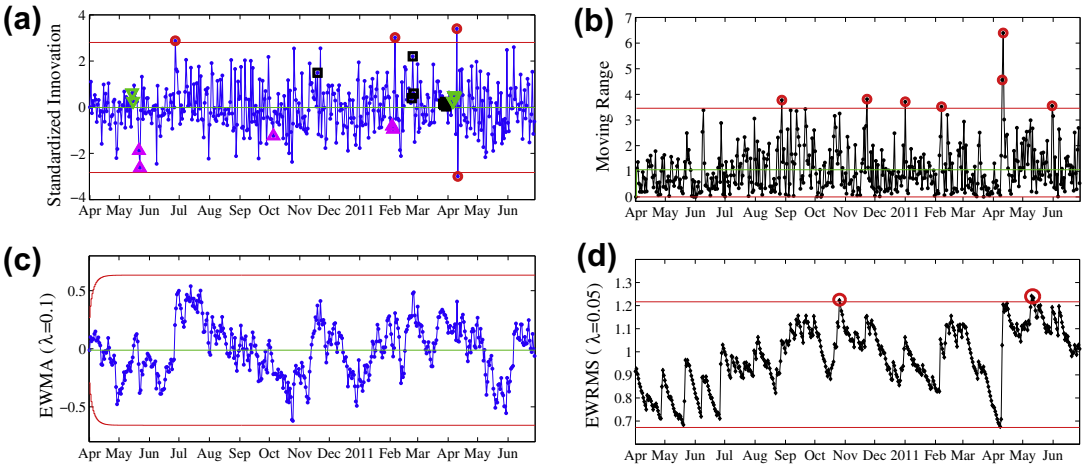

Fig. 10. Control charts for Displ-L: (a) individual, (b) moving range, (c) EWMA, (d) EWRMS.

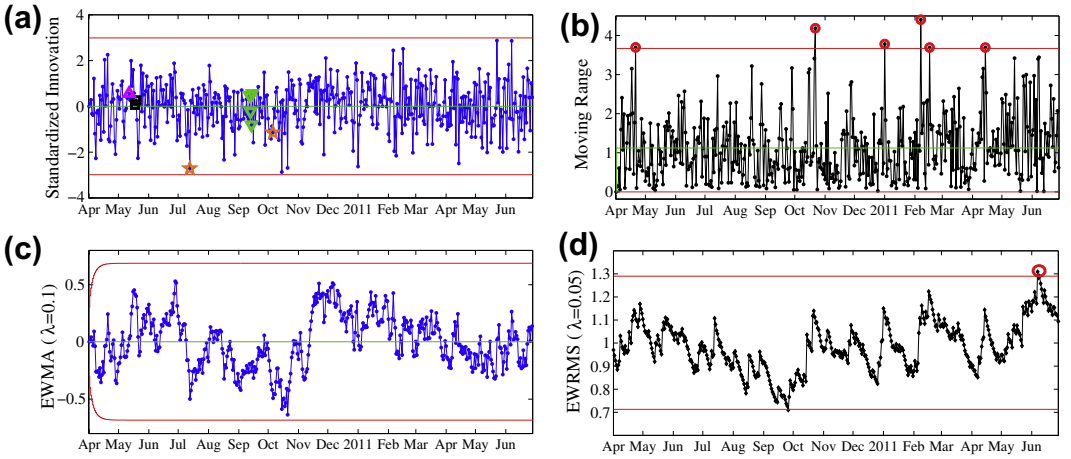

Fig. 11. Control charts for G1-S2-M: (a) individual, (b) moving range, (c) EWMA, (d) EWRMS.

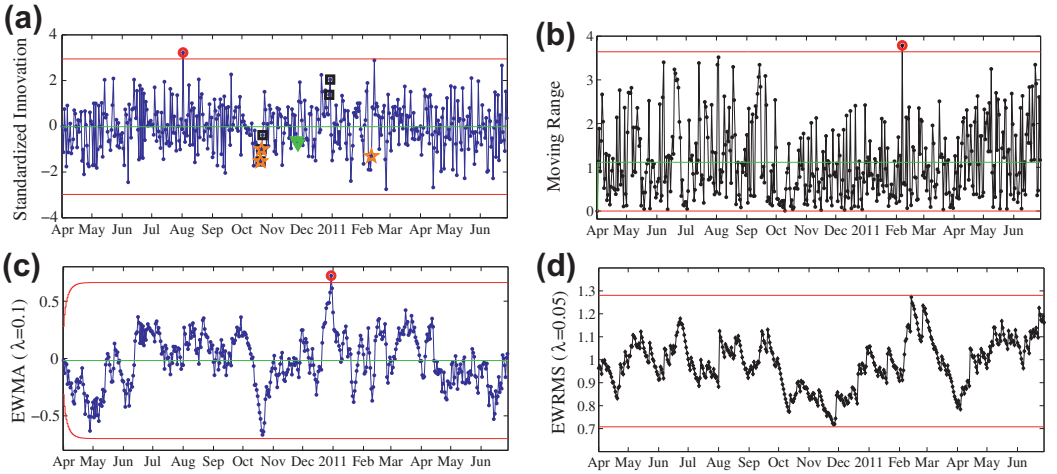

Fig. 12. Control charts for G4-P2-TF: (a) individual, (b) moving range, (c) EWMA, (d) EWRMS.

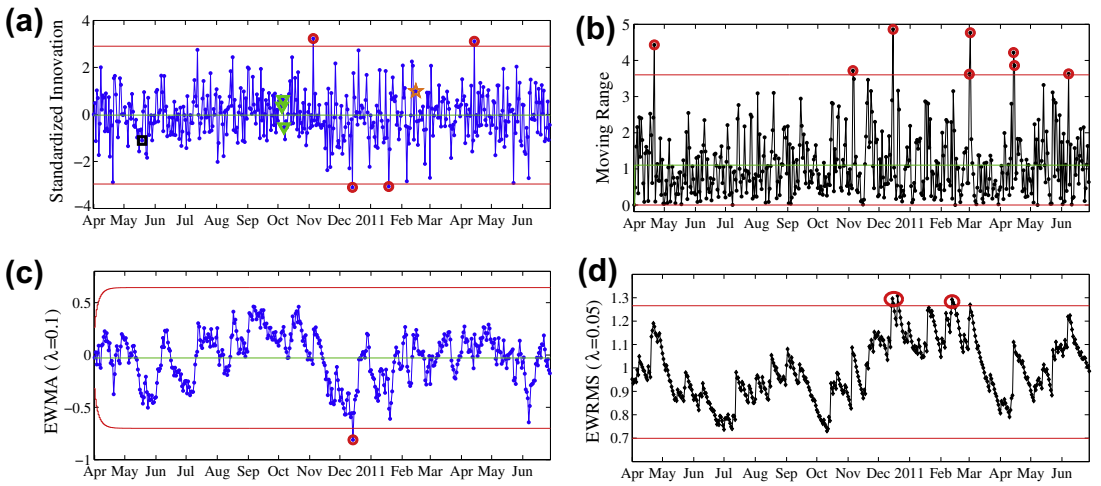

Fig. 13. Control charts for G4-WCP-ST: (a) individual, (b) moving range, (c) EWMA, (d) EWRMS.

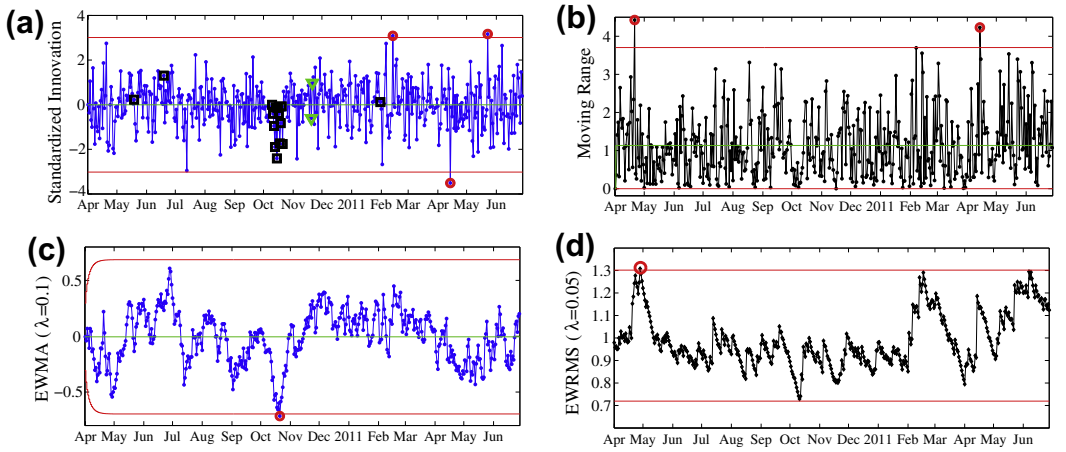

Fig. 14. Control charts for G4-S2-M: (a) individual, (b) moving range, (c) EWMA, (d) EWRMS.

Fig. 14 for G4-S2-M. We also collect and summarize the results of our analysis of special-cause variation. Specifically, we detect and characterize salient events whose effect is unexplained by the the statistical models presented earlier.

Table 4 presents a summary of the events detected. We record their duration and classify them as either transitory/outliers or persistent shifts/drifts, and arrange them in chronological order. We also record the physical nature of the respective measurements, as well as the control charts in which each event is detected. For example, "I (n2, n6), EWMA" means that the Individual Control Chart with rules N2 and N6, as well as the EWMA Control Chart signaled the event.

The results in Table 4 provide a record of 43 possible special-cause events. More than half of these events correspond to persisting shifts or drifts in the mean or variance of the measurement series – lasting at least 3 days. The remaining events correspond to outliers detected by the Shewhart Control Charts. In terms of assessing the results:

- Following the discussion in Section 3.2.2, application of the Individual Control Charts with the supplementary runs rules would be expected to yield ≈46 possible events ($6 \times 455 \times 0.0169$), and thus, it appears that the number of signals is reasonable. If anything, the results suggest overestimation of the variances in the measurement sequences, resulting in underdetection of possible special-cause events. This, in turn, increases the confidence with which the detected events can be attributed to special causes (as opposed to random variation), i.e., it is akin to increasing L, which decreases the Type I error, α.
- In terms of the reliability of the results, we observe that several of the most salient events (by their duration) were detected by multiple sensors in different locations, which also increases the confidence with which detected events can be attributed to special causes. This observation also increases the confidence with which such events can be related to the bridge's structural response, as opposed to loss of calibration of the sensors or other special causes.

Table 4
Summary of special-cause events detected from the six sampled distresses.

Event type	Date	Duration (days)	Inference	Measurement	Control charts
Mean shifts or drifts			Tension	G1-S2-M	I (n2, n3)
	2010.05.10	11	Tension	G4-S2-M	I (n2)
			Compression	G4-WCP-ST	I (n2)
	2010.05.17	7	*G1 drifted west*	Displ-L	I (n3)
	2010.06.12	9	Tension	G4-S2-M	I (n2)
	2010.07.10	5	*Compression*	G1-S2-M	I (n6)
	2010.10.01	6	*G1 drifted west*	Displ-L	I (n3)
	2010.10.03	5	*Compression*	G1-S2-M	I (n6)
				G1-S2-M	I (n2), EWMA
	2010.10.14	7–9	*Compression*	G4-P2-TF	I (n2)
	2010.10.16	5	*Compression*	G4-P2-TF	I (n6)
	2010.12.15	10	*G1 shifted south*	Displ-T	I (n2)
	2010.12.23	10	Tension	G4-P2-TF	I (n2)
	2011.01.24	9	Tension	G4-S2-M	I (n2)
	2011.01.27	7	*G1 drifted west*	Displ-L	I (n3)
		8–10	*G1 shifted south*	Displ-T	I (n2, n6), EWMA
	2011.02.08	4	*Compression*	G4-P2-TF	I (n6)
	2011.02.12	5	Tension	G4-WCP-ST	I (n6)
	2011.02.17	9			
	2011.03.20	10	G1 shifted east	Displ-L	I (n2)
	2011.03.27	7	G1 drifted south		
	2011.05.19	6	G1 drifted north	Displ-T	I (n3)
Variance shifts or drifts	2010.04.03	2	Volatile movement	Displ-T	MR, I
	2010.12.15	8	Volatile strain	G4-WCP-ST	EWRMS, EWMA, I
		7	Volatile movement	Displ-T	EWRMS
	2011.02.13	4	Volatile strain	G4-WCP-ST	EWRMS
	2011.02.25	6	Volatile movement	Displ-T	EWRMS
	2011.04.12	3–4	Volatile movement	Displ-T	EWRMS
	2011.05.10	3	Volatile movement	Displ-L	EWRMS
			Volatile strain	G1-S2-M	EWRMS
	2011.06.09	3–4	Volatile movement	Displ-T	EWRMS, I
Outliers in mean	2010.04.16	1	G1 moved to north	Displ-T	I
	2010.08.03	1	Tension	G4-P2-TF	I
	2010.11.06	1	Tension	G4-WCP-ST	I, MR
	2011.01.01	1	G1 moved to north	Displ-T	I, MR
	2011.01.20	1	*Compression*	G4-WCP-ST	I
	2011.02.14	1	Tension	G4-S2-M	I
			G1 moved to east	Displ-L	I, MR
	2011.04.11	2	G1 moved to north	Displ-T	I, MR
			Compression	G4-S2-M	I, MR
	2011.04.15	1	Tension	G4-WCP-ST	I, MR
	2011.05.24	1	Tension	G4-S2-M	I
Outliers in variance				G1-S2-M	MR
	2010.04.22	1	Volatile strain	G4-S2-M	MR
				G4-WCP-ST	MR
	2010.09.13	2	Volatile G1 movement	Displ-L	MR
	2010.10.23	1	Volatile strain	G1-S2-M	MR
	2011.01.02	1	Volatile strain	G1-S2-M	MR
				G1-S2-M	MR
	2011.02.08	1	Volatile strain	G4-P2-TF	MR
	2011.02.17	1	Volatile strain	G1-S2-M	MR
	2011.03.02	2	Volatile strain	G4-WCP-ST	MR
	2011.05.01	1	Volatile G1 movement	Displ-T	MR
	2011.06.10	1	Volatile strain	G4-WCP-ST	MR

- In general, combining control charts can improve the efficiency and the reliability of the signals. For example, I (n2) requires 9 observations, whereas EWMA may only need 4 or 5. Simultaneously, in terms of reliability, an outlier can result in EWMA signals, but is less likely to trigger signals in I (n2). The results display the overlap between the different control charts and supplementary runs rules.

In an online monitoring context, detection of the aforementioned events would provide a rigorous statistical basis to react to measurements that do not conform to those collected under ordinary conditions, and thus, support (equipment or structural) inspections, road closures, etc. *Post-hoc* detection of special-cause events supports forensic analysis of (major damage) events. For example, it can, conceivably, provide indication of precursor, extraordinary events. From a modeling perspective,

Table A.5
Variance inflation factor.

VIF	Linear trend	Humidity	Steel temperature	Air temperature	Benchmark
Full model	1.25	1.13	80.92	79.73	> 10
Partial model	1.21	1.12	1.23	Removed	

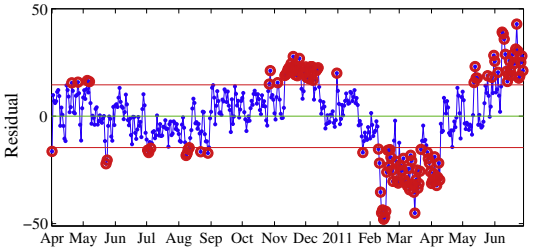

Fig. 15. Individual control chart for Displ-T regression residuals.

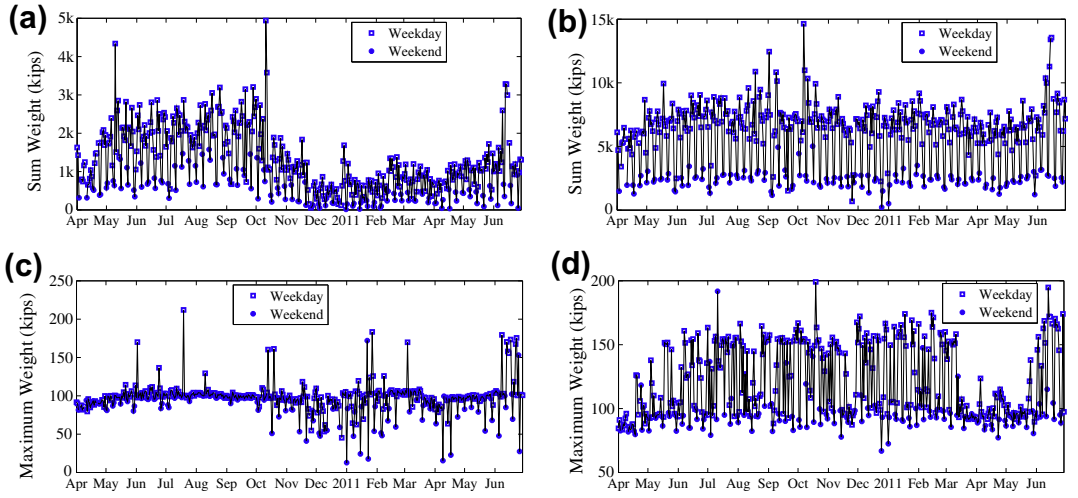

Fig. 16. Daily traffic weight: (a) left lane sum, (b) right lane sum, (c) left lane maximum, (d) right lane maximum.

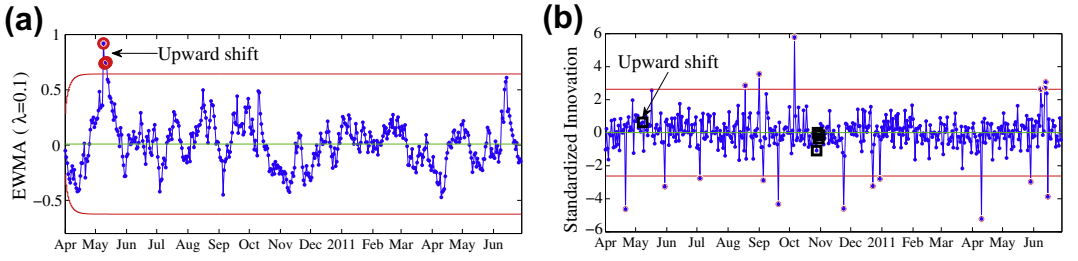

Fig. 17. Control chart for daily cumulative traffic weight: (a) EWMA (left lane, $\lambda = 0.1$), (b) individual (right lane, Nelson Rule N2).

post hoc detection of special-cause events provides guidance to refine the statistical models (used to explain and predict common-cause variation), i.e., to exclude (explained) outliers (Montgomery, 2009), or to use intervention analysis to characterize events whose effect is persistent/permanent (Box and Tiao, 1975; Chu and Durango-Cohen, 2008b). Referring to the results, while there is little evidence of deterioration (or other permanent changes) not adequately explained by the statistical models of common-cause variation, exclusion of (a subset of) measurements associated with special-cause events could lead to refinements, i.e., decreases in the variance estimates.

To illustrate the process of identifying sources of special-cause variation, in C we consider the effect of traffic loading. We found that a sustained increase in the seasonally-adjusted traffic load coincides with the event with the longest duration (11 days beginning on May 10, 2010). This event resulted in unexplained strain measurements at various locations and may have also contributed to longitudinal displacement. Unfortunately, similar links were not established to explain other events, highlighting the difficulty to identify *assignable causes*.

5. Conclusions

In this paper we develop an integrated, generally-applicable statistical framework that links infrastructure performance modeling and statistical process control to support safe and efficient management and operations of transportation infrastructure. Fundamentally, the framework contributes a methodological link between the literature on SHM, and on statistical performance modeling to support transportation infrastructure/asset management.

The framework consists of two parts: development of statistical models to explain, predict and control for common-cause variation; that is, changes that can be attributed to usual operating conditions (with effects throughout the data); and use of control charts to detect special-cause or unusual events. In addition to describing the methodology in detail and position the work in relation to the literature, we use the framework to process strain and displacement data from the SHM system installed on the Hurley Bridge. The data were collected from April 1, 2010 to June 29, 2011. Our implementation of the first part of the framework consists of estimation of regression models to control for variability in the measurements that can be related to changes in exogenous variables, as well as estimation of ARIMA-GARCH models, a class of time series models, to control for serial dependence, a significant source of common-cause variation, in the regression residuals. Our analysis shows that:

- Seasonal effects, i.e., temperature and humidity, and a linear trend, included as a supplementary predictor, account for a large percentage (40–90%) of the overall variation in the response measurements.
- Small, but significant, linear trends indicate permanent displacement of the bridge, i.e., after controlling for seasonal variations, the net position is drifting. This is likely an indication of deterioration of the bridge supports. Linear trends in the strain measurements could be influenced by changes in the materials, i.e., fatigue, sensors or traffic loads.
- There is evidence that serial dependence, i.e., carryover effects, is a significant source of common-cause variation.

Our implementation of the second part of the framework uses Shewhart (Individual and Moving Range) and Memory Control Charts to analyze special-cause variation not explained by the aforementioned statistical models. The analysis detected 43 possible special-cause events. Events occurring on May 10–20, June 12–20, October 14–20 of 2010, and January 24–31, February 8–16 of 2011, are worthy of additional investigation due to their significance, duration and magnitude. To illustrate the process of identifying sources of special-cause variation, we consider the effect of traffic loading, and found that the event in May 10–20, 2010 coincides with a sustained increase in the seasonally-adjusted traffic load. Unfortunately, similar links for other events were not established, highlighting the difficulty in identifying sources of special-cause variation – a limitation of SPC.

Limitations of the present study include:

- The homogeneous temporal resolution of the measurements (daily averages) may lead to (short-term) loss of information. In part, the problem originates from the data collection protocols, which result in the transmission and recording of hourly averages. Ideally, the temporal resolution ought to be tailored for different distresses to match their physical nature and reflect managerial concerns;
- In the same spirit, while the use of commonly-specified statistical models is adequate (to control for common-cause variation and detect special-cause events), ideally, specifications should be tailored to the measurements;
- The sequential estimation of linear regression and time series models may introduce bias to the estimation results in a strict sense. Although this is common in practical applications, one needs to be aware and careful of its negative implications. The adoption of state-space specifications of time series models as in Chu and Durango-Cohen (2007) seems like a promising approach to address this problem;
- Among other advantages, additional data availability (beyond the 15 months used in the present study) would provide an opportunity to test the framework's online monitoring capabilities. As is done in online applications of SPC (cf. Montgomery, 2009), the analysis period would be divided into two phases: a calibration phase that would allow for the estimation of performance models to control for common-cause variation; and a control/monitoring phase dedicated to special-cause event detection.

Acknowledgments

The authors acknowledge the technical support of David Kosnik from the Infrastructure Technology Institute at Northwestern University, and are grateful for the substantive and constructive feedback provided by two anonymous referees.

The research was supported by grants from the Infrastructure Technology Institute, and from the National Science Foundation.

Appendix A. Multicolinearity

In multilinear regressions, highly correlated predictors have the potential to yield erratic coefficient estimates, and unreliable predictions. This phenomenon is referred to as multicolinearity. We employ a Variance Inflation Factor (VIF), Eq. (A.1), to evaluate its effect.

$$\mathrm{VIF}_j = \frac{1}{1 - R_j^2} \tag{A.1}$$

where R_j^2 is the coefficient of determination of a regression of predictor j using all other predictors. A VIF value at or above 10 indicates a multicolinearity problem, and the corresponding predictor is eliminated from the regression model. Table A.5 presents the VIF's of each variable in the empirical study in Section 4.2.1. The analysis led to the removal of ambient temperature from the regression models.

Appendix B. Control charts applied to regression residuals

To illustrate the pitfalls of implementations of Shewhart control charts to correlated measurements, Fig. 15 shows an Individual Control Chart to monitor the regression residuals. Comparison with Fig. 6(a) highlights the (negative) impact of serial dependence, which violates the assumption of random variation, and leads to 130 signals over 455 measurements. This example is consistent with those presented in Alwan and Roberts (1988) and others.

Appendix C. Traffic loading

We analyzed traffic loading on both lanes of the Hurley Bridge as a factor contributing to its deterioration. Although the entire series of cumulative and maximum traffic loading (Fig. 16) turned out to be statistically insignificant in the regression model in Section 4.2.1, we found temporal consistency that connects its unusual (persisting) shift with the longest-lasting special-cause event (Table 4).

We treated each sequence of traffic data in Fig. 16 as a dependent measurement and followed the methodology in Section 3 to account for common-cause effects (with an additional dummy variable in regression to adjust for strong weekly patterns). Besides a few outliers, the EWMA Chart and Individual Chart with runs rule N2 (Fig. 17), respectively, signaled a persisting upward shift in the daily cumulative traffic weight on each lane over the second week of May, 2010. This overlaps with the unusual tension in the mid-span of Girder 1 and Girder 4 which lasted 11 days combined with a 7-day-long westbound drift of Girder 1. Given the small chance of such a coincidence, it is reasonable to infer plausible link between the heavy traffic and these extreme events. It is worth noting that such a link is informative, thus providing a direction for further study, rather than conclusive. We also note that we have not identified links to other events.

References

AASHO, 1962. The AASHO Road Test, highway Research Board Special Report 73, National Academy of Sciences, National Research Council, Washington, DC.
Alwan, L., 2000. Statistical Process Analysis. McGraw-Hill, New York, NY.
Alwan, L., Roberts, H., 1988. Time-series modeling for statistical process control. Journal of Business & Economic Statistics 6 (1), 87–95.
Archilla, A.R., Madanat, S., 2000. Development of pavement rutting model from experimental data. Journal of Transportation Engineering 126 (4), 291–299.
Balageas, D., Fritzen, C.-P., Güemes, A., 2006. Structural Health Monitoring. ISTE Ltd., London, United Kingdom.
Box, G., Tiao, G., 1975. Intervention analysis with applications to economic and environmental problems. Journal of the American Statistical Association 70 (349), 70–79.
Brockwell, P., Davis, R., 2002. Introduction to Time Series and Forecasting. Springer-Verlag.
Chen, Y., 2013. A Statistical Health-Monitoring Framework for Transportation Infrastructure. Ph.D. thesis, Northwestern University.
Chu, C.-Y., Durango-Cohen, P., 2007. Estimation of infrastructure performance models using state-space specifications of time series models. Transportation Research Part C 15 (1), 17–32.
Chu, C.-Y., Durango-Cohen, P., 2008a. Estimation of dynamic performance models for transportation infrastructure using panel data. Transportation Research Part B 42 (1), 57–81.
Chu, C.-Y., Durango-Cohen, P., 2008b. Incorporating maintenance effectiveness in the estimation of dynamic infrastructure performance models. Computer-Aided Civil and Infrastructure Engineering 23 (3), 174–188.
Crowder, S., 1987. Computation of ARL for combined individual measurement and moving range charts. Journal of Quality Technology 19 (2), 98–102.
Crowder, S., 1989. Design of exponentially weighted moving average schemes. Journal of Quality Technology 21 (3), 155–162.
Deming, W., 1975. On probability as a basis for action. The American Statistician 29 (4), 146–152.
Doebling, S., Farrar, C., Prime, M., 1998. A summary review of vibration-based damage identification methods. The Shock and Vibration Digest 30 (2), 91–105.
Duncan, A.J., 1986. Quality Control and Industrial Statistics, 5th ed. Richard D. Irwin, Homewood, IL.
Engle, R., 2001. GARCH 101: The use of ARCH/GARCH models in applied econometrics. Journal of Economic Perspectives 15 (4), 157–168.
Fang, Y., Zhang, J., 1999. Performance of control charts for autoregressive conditional heteroscedastic processes. Journal of Applied Statistics 26 (6), 701–714.
Farrar, C., Worden, K., Mansin, G., Park, G., 2005. Fundamental axioms of structural health monitoring. In: Proceedings of the 5th International Workshop on Structural Health Monitoring, Stanford, CA.

Frangopol, D., Kong, J., Gharaibeh, E., 2001. Reliability-based management of highway bridges. Journal of Computing in Civil Engineering 15 (1), 27–34.
Friswell, M., Mottershead, J., 1995. Finite Element Model Updating in Structural Dynamics. Kluwer Academic Publishers, Amsterdam, The Netherlands.
Fritzen, C.-P., 2005. Vibration-based structural health monitoring – concepts and applications. Key Engineering Materials 293–294, 3–20.
Fugate, M., Sohn, H., Farrar, C., 2001. Vibration-based damage detection using statistical process control. Mechanical Systems and Signal Processing 15 (4), 707–721.
Gendreau, M., Soriano, P., 1998. Airport pavement management systems: an appraisal of existing methodologies. Transportation Research Part A 32 (3), 197–214.
Hudson, W., Haas, R., Uddin, W., 1997. Infrastructure Management. McGraw-Hill, New York, NY.
Johnson, E.H.L., Katafygiotis, L., Beck, J., 2004. Phase I IASC–ASCE structural health monitoring benchmark problem using simulated data. Journal of Engineering Mechanics 130 (1), 3–15.
Kiremidjian, A., 2009. Statistical Pattern Recognition. Wiley, West Sussex, United Kingdom.
Kosnik, D., 2010. Structural health monitoring of Wisconsin Structure B-26-7 Westbound USH-2 over the Montreal River – Hurley, Wisconsin. Installation Report, Northwestern University
Li, Z., Chan, T., Ko, J., 2001. Fatigue analysis and life prediction of bridges with structural health monitoring data – Part 1: Methodology and strategy. International Journal of Fatigue 23, 45–53.
Lucas, J., Saccucci, M., 1990. Exponentially weighted moving average schemes: Properties and enhancements. Technometrics 32 (1), 1–12.
Lynch, J., 2007. An overview of wireless structural health monitoring for civil structures. Philosophical Transactions of The Royal Society Series A 365 (1851), 345–372.
Lynch, J., Wang, Y., Loh, K., Yi, J.-H., Yun, C.-B., 2006. Performance monitoring of the Geumdang bridge using a dense network of high-resolution wireless sensors. Smart Materials and Structures 15 (6), 1561–1575.
Madanat, S., Mishalani, R., Wan Ibrahim, W.H., 1995. Estimation of infrastructure transition probabilities from condition rating data. Journal of Infrastructure Systems 1 (2), 120–125.
Madanat, S., Wan Ibrahim, W.H., 1995. Poisson regression models of infrastructure transition probabilities. Journal of Transportation Engineering 121 (3), 267–272.
Madanat, S., Karlaftis, M., McCarthy, P., 1997. Probabilistic infrastructure deterioration models with panel data. Journal of Infrastructure Systems 3 (1), 4–9.
Mandel, B., 1969. The regression control chart. Journal of Quality Technology 1 (1), 1–9.
McNeil, S., Markow, M., Neumann, L., Ordway, J., Uzarski, D., 1992. Emerging issues in transportation facilities management. Journal of Transportation Engineering 118 (4), 477–495.
Mishalani, R., Madanat, S., 2002. Computation of infrastructure transition probabilities using stochastic duration models. Journal of Infrastructure Systems 8 (4), 139–148.
Montgomery, D., 2009. Introduction to Statistical Quality Control. Wiley, Hoboken, NJ.
Nair, K., Kiremidjian, A., 2007. Time series based structural damage detection algorithm using Gaussian mixture modeling. Journal of Dynamic Systems, Measurement and Control 129 (3), 285–293.
Nelson, L., 1984. Technical aids: The shewhart control chart–tests for special causes. Journal of Quality Technology 16 (4), 238–239.
Ord, J., Koehler, A., Snyder, R., Hyndman, R., 2009. Monitoring processes with changing variances. International Journal of Forecasting 25 (3), 518–525.
Prozzi, J., Madanat, S., 2001. Nonlinear model for predicting pavement performance before and after rehabilitation. Proceedings of the Second International Symposium on Maintenance and Rehabilitation of Pavements and Technological Control. Auburn, AL.
Rice, J., Mechitov, K., Sim, S., Spencer, B., Agha, G., 2011. Enabling framework for structural health monitoring using smart sensors. Structural Control and Health Monitoring 18 (5), 574–587.
Shewhart, W., 1931. Economic Control of Quality of Manufactured Products. Van Nostrand Company, New York, NY.
Sohn, H., Farrar, C., Hemez, F., Czarnecki, J., 2002. A review of structural health monitoring literature 1996–2001. Journal of Structural Engineering, Technical Report LA-UR-02-2095. Los Alamos National Laboratory.
Sohn, H., Fugate, M., Farrar, C., 2000. Damage diagnosis using statistical process control. In: Proceedings of the 7th International Conference on Recent Advances in Structural Dynamics. Southampton, United Kingdom.
Van Noortwjk, J., Frangopol, D., 2004. Deterioration and maintenance models for insuring safety of civil infrastructures at lowest life-cycle cost. In: Frangopol, D.M., Brühwiler, E., Faber, M.H., Adey, B. (Eds.), Life-cycle Performance of Deteriorating Structures: Assessment, Design and Management. American Society of Civil Engineers, Reston, VA, pp. 384–391.
Vincent, G., 1962a. Correlation of predicted and observed suspension bridge behavior. Transactions of the American Society of Civil Engineers 127 (PII), 646–666.
Vincent, G., 1962b. Golden gate bridge vibration studies. Transactions of the American Society of Civil Engineers 127 (2), 667–707.
Wenzel, H., 2009. Health Monitoring of Bridges. Wiley, West Sussex, United Kingdom.
Wowk, V., 1991. Machinery Vibration Measurement and Analysis. McGraw-Hill, New York, NY.
Xu, Y., Ko, J., Zhang, W., 1997. Vibration studies of Tsing Ma suspension bridge. Journal of Bridge Engineering 2 (4), 149–156.